

Topological metal-insulator transitions in one-dimensional non-Hermitian quasicrystals: beyond \mathcal{PT} -symmetry

Guangjie Zhang,^{1,*} Bing Shao,^{1,*} Longwen Zhou,^{1,2,3,†} Jiangbin Gong,^{4,5,6,‡} and Weiwei Zhu^{7,§}

¹College of Physics and Optoelectronic Engineering,
Ocean University of China, Qingdao 266100, China

²Qingdao Key Laboratory of Advanced Optoelectronics, Qingdao 266100, China

³Engineering Research Center of Advanced Marine Physical Instruments and Equipment of MOE, Qingdao 266100, China

⁴Department of Physics, National University of Singapore, 117551, Singapore

⁵Centre for Quantum Technologies, National University of Singapore, 117543, Singapore

⁶MajuLab, CNRS-UCA-SU-NUS-NTU International Joint Research Unit, Singapore.

⁷Center for Phononics and Thermal Energy Science, China-EU Joint Lab on Nanophononics,
Shanghai Key Laboratory of Special Artificial Microstructure Materials and Technology,
School of Physics Science and Engineering, Tongji University, Shanghai 200092, China

One-dimensional non-Hermitian quasicrystals with parity and time-reversal (\mathcal{PT}) symmetry can simultaneously exhibit localization-delocalization transition, topological phase transition, and \mathcal{PT} -symmetry-breaking transition. This motivates this work to investigate how the absence of \mathcal{PT} symmetry impacts topological metal-insulator transitions in non-Hermitian quasicrystals. We propose a non-Hermitian quasiperiodic model that generally does not preserve \mathcal{PT} symmetry and demonstrate that, in most parameter regions, such a system supports triple phase transitions that encompass localization, topology, and degeneracy-breaking. The system may also exhibit a particular type of localization-delocalization transition analogous to the Hermitian case, namely, without activating topological phase transitions or degeneracy-breaking transitions. Our work extends the topological metal-insulator transitions previously studied in \mathcal{PT} -symmetric systems to a more general class of non-Hermitian setting, and further reveals that non-Hermitian systems can host distinct types of localization behavior.

I. INTRODUCTION

Quasiperiodic systems, which are not periodic but possess long-range order, offer a clean and controllable platform for investigating metal-insulator transitions [1–3] and exploring a wide variety of topological phases [4–6] in one dimension, where arbitrarily weak uncorrelated disorder leads to Anderson localization [7] and only a limited set of pristine topological phases can exist [8]. This is largely because quasiperiodic systems can often be obtained through dimensional reduction from higher-dimensional periodic structures. A paradigmatic example is the one-dimensional (1D) Aubry-André-Harper (AAH) model [9], which emerges from dimensional reduction of the Hofstadter model [10]. Inheriting features from its two-dimensional parent, the AAH model and its generalizations exhibit rich metal-insulator transitions and topological phases. In addition, quasiperiodic disorder has been utilized to realize topological Anderson insulators, which support gapped topological edge states that coexist with critical or extended bulk states [11–13]. This behavior contrasts with the conventional disorder-induced topological Anderson insulator [14–16], which typically features gapless topological edge states and a fully localized bulk.

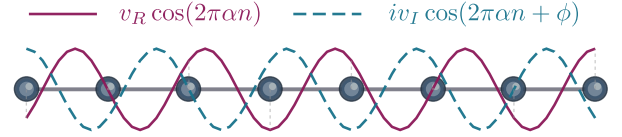


FIG. 1. Real and imaginary parts of onsite potential in a one-dimensional non-Hermitian quasicrystal, both following a cosine modulation but with a relative phase shift ϕ .

Non-Hermitian systems exhibit richer localization and topological phenomena than their Hermitian counterparts [17–20] even in one spatial dimension. Under open boundary conditions, bulk eigenstates can become edge-localized due to non-Hermitian skin effects (NHSEs) [21–24], in addition to conventional Anderson localization. Moreover, non-Hermitian systems can host metal-insulator transitions in one dimension under periodic boundary conditions [25–28], as exemplified by the disordered Hatano-Nelson model [29–31]. Non-Hermitian systems also support a broader range of topological phases than Hermitian systems, including both point-gapped and line-gapped topological states. According to the Bernard-LeClair symmetry classification [32–34], non-Hermitian systems fall into 38 distinct symmetry classes, revealing a richer topological landscape than Hermitian systems.

The combination of quasiperiodic and non-Hermitian modulations is expected to generate unique localization and topological phenomena that are absent in either Hermitian quasicrystals or non-Hermitian crystals. Various

* These authors contributed equally to this work.

† zhoulw13@u.nus.edu

‡ phygj@nus.edu.sg

§ phyzhuw@tongji.edu.cn

types of such non-Hermitian quasicrystals (NHQCs) have been investigated [35–54], revealing a wealth of intriguing behavior, including \mathcal{PT} -symmetry-breaking transitions, topological phase transitions, and non-Hermitian mobility edges [55–72]. Among these, the topological triple phase transition [73–75] has attracted particular attention due to the simultaneous occurrence of localization, topological, and \mathcal{PT} -symmetry-breaking transitions. However, most existing studies are restricted to \mathcal{PT} -symmetric systems, and the behavior in more general non-Hermitian settings remains largely unexplored.

In this paper, we introduce an NHQC model in which the real and imaginary parts of the onsite potential are subject to the same cosine modulation with a relative phase shift ϕ (Fig. 1). In general, the model does not preserve the \mathcal{PT} symmetry, except at special values $\phi = m\pi + \pi/2$ with $m \in \mathbb{Z}$. We demonstrate that the model can simultaneously exhibit localization and topological transitions by tuning either the modulation amplitude or the relative phase shift, a phenomenon that we termed the topological metal-insulator transition. Furthermore, we show that the system undergoes a degeneracy-breaking transition—from twofold degenerate to non-degenerate in its spectrum—which is more general than the \mathcal{PT} transition. Both the topological and degeneracy-breaking transitions originate from the NHSEs in momentum space, manifested there as asymmetric couplings. We also investigate phase transitions at special values $\phi = m\pi + \pi/2$, where the system preserves \mathcal{PT} symmetry, and at $\phi = m\pi$, where asymmetric couplings in momentum space vanish. At $\phi = m\pi + \pi/2$, the system exhibits a quartet phase transition that involves localization, topology, degeneracy-breaking and \mathcal{PT} -breaking. At $\phi = m\pi$, only the localization transition remains. Therefore, we identify two distinct types of Anderson localization in 1D NHQCs: one originating from topology unique to non-Hermitian systems, and the other analogous to that in Hermitian setups.

The rest of the paper is organized as follows. In Sec. II, we introduce our model and the quantities to characterize its localization properties, including the inverse participation ratio (IPR) and the fractal dimension (FD). In Sec. III, we examine the triple phase transition of localization, topology, and degeneracy-breaking by investigating IPRs, winding numbers, and degeneracy rates in the parameter space of the system. In Sec. IV, we study the localization properties of the system at specific values $\phi = m\pi + \pi/2$ and $\phi = m\pi$ of the phase shift. We conclude our study and discuss potential future work in Sec. V.

II. MODEL AND METHODS

We consider a 1D lattice model as illustrated in Fig. 1, which is described by the tight-binding Hamiltonian

$$H = \sum_n \left(t a_{n+1}^\dagger a_n + \text{H.c.} \right) + \sum_n V_n a_n^\dagger a_n, \quad (1)$$

where a_n (a_n^\dagger) denotes the annihilation (creation) operator at the lattice site n , t is the nearest-neighbor hopping amplitude, and V_n represents a complex quasiperiodic onsite potential of the form

$$V_n = v_R \cos(2\pi\alpha n) + i v_I \cos(2\pi\alpha n + \phi). \quad (2)$$

Here, α is an irrational number chosen to be $(\sqrt{5} - 1)/2$ that ensures quasiperiodicity, while v_R , v_I , and ϕ denote the real amplitude, imaginary amplitude, and relative phase shift of the modulations, respectively. In general, the model does not preserve \mathcal{PT} symmetry except at special parameter values, e.g., $\phi = m\pi + \pi/2$ with $m \in \mathbb{Z}$.

Under duality transformation $a_n = \frac{1}{\sqrt{L}} \sum_k b_k e^{i2\pi\alpha kn}$, the Hamiltonian in Eq. (1) can be transformed into momentum space, yielding

$$H_k = \sum_k \left(J_+ b_{k+1}^\dagger b_k + J_- b_k^\dagger b_{k+1} \right) + \sum_k \tilde{V}_k b_k^\dagger b_k. \quad (3)$$

Here, b_k (b_k^\dagger) is the annihilation (creation) operator at quasimomentum k . In this form, non-Hermiticity works as asymmetric nearest-neighbor couplings $|J_+| \neq |J_-|$. The onsite modulation becomes Hermitian, as given by the real function \tilde{V}_k . Explicitly, the system parameters are

$$\begin{aligned} J_+ &= \left(\frac{v_R}{2} - \frac{v_I}{2} \sin \phi \right) + i \frac{v_I}{2} \cos \phi, \\ J_- &= \left(\frac{v_R}{2} + \frac{v_I}{2} \sin \phi \right) + i \frac{v_I}{2} \cos \phi, \\ \tilde{V}_k &= 2t \cos(2\pi\alpha k). \end{aligned} \quad (4)$$

In general, asymmetric couplings $|J_+| \neq |J_-|$ give rise to NHSEs, while onsite modulation \tilde{V}_k drives metal-insulator transitions. The interplay of these ingredients—nonreciprocal hoppings and quasiperiodic potential—leads to phenomena richer than those produced by either alone, such as asymmetric localized states [37] and topological triple phase transitions [73–75]. The models in Eqs. (1) and (3) are mutually dual and exhibit complementary localization behaviors. Therefore, we expect that the model in Eq. (1) also hosts rich localization and topological features. Moreover, analyzing the dual model in Eq. (3) provides a useful approach to understanding the physics of the system in Eq. (1).

Before presenting our main results, we first introduce the quantities used to characterize the localization properties of the system, namely the IPR and the FD. In numerical calculations, we adopt a rational approximation $\alpha \approx F_m/F_{m+1} \equiv \alpha_m$ and set the size of the system to $L = F_{m+1}$, where F_m denotes the m th Fibonacci number defined recursively by $F_{m+1} = F_{m-1} + F_m$ with $F_1 = F_2 = 1$. This choice allows us to impose periodic boundary conditions and thereby avoid boundary-related artifacts.

The IPR of the i th right-normalized eigenstate $|\Psi_i\rangle = \sum_{n=1}^L \psi_{i,n} a_n^\dagger |\text{vac}\rangle$ of H is defined as

$$\text{IPR}_i = \sum_{n=1}^L |\psi_{i,n}|^4, \quad (5)$$

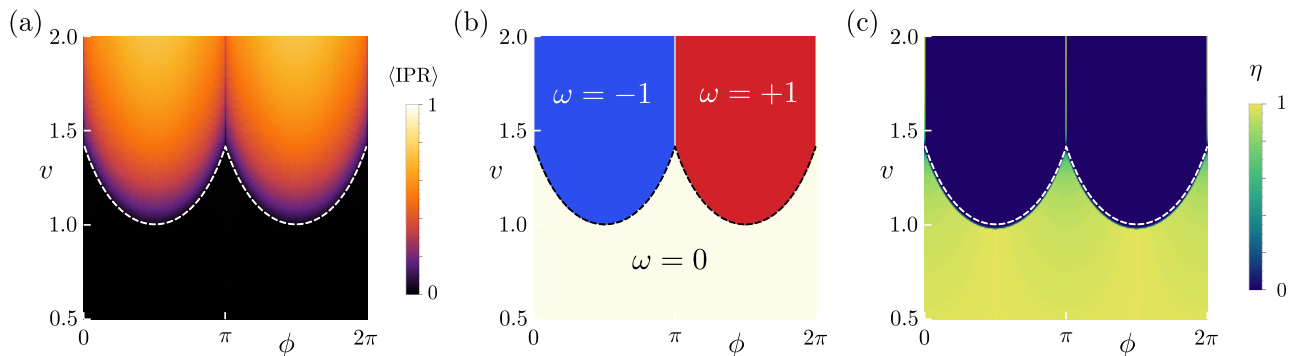


FIG. 2. Phase diagrams for topological triple phase transitions. (a) Localization phase diagram: averaged IPR, $\langle \text{IPR} \rangle$, as a function of v and ϕ . Dark (bright) regions correspond to extended (localized) phases. (b) Topological phase diagram: winding number ω as a function of v and ϕ . (c) Degeneracy phase diagram: degeneracy rate η as a function of v and ϕ . In numerical simulations, the system size is set to $L = F_{15} = 610$. Two eigenenergies E_1 and E_2 are considered degenerate if their distance $|\delta E| \equiv |E_1 - E_2|$ is less than 10^{-5} . Dashed lines denote phase boundaries obtained analytically.

which goes to 1 for a localized state and to 0 for an extended state when $L \rightarrow \infty$. The FD is further given by

$$\Gamma \equiv \text{FD}_i = - \lim_{L \rightarrow \infty} \frac{\ln \text{IPR}_i}{\ln L}, \quad (6)$$

which approaches 0 in localized phases and 1 in extended phases for all $i = 1, \dots, L$. We also examine the averaged IPR, defined as

$$\langle \text{IPR} \rangle = \frac{1}{L} \sum_{i=1}^L \text{IPR}_i, \quad (7)$$

which approaches 1 in localized regimes and 0 in extended regimes. Throughout this work, we set $t = 1$ and $v_R = v_I = v$ unless otherwise stated.

III. PHASE TRANSITIONS

In this section, we examine localization, topological, and degeneracy-breaking phase transitions driven by the amplitude and phase shift of the onsite potential in our system. We demonstrate that the three distinct transitions coincide and arise along the same boundary in parameter space.

A. Localization-delocalization transitions

We first investigate the localization properties of the system by computing the averaged IPR, $\langle \text{IPR} \rangle$, as a function of v and ϕ . The results are shown in Fig. 2(a). Extended phases are characterized by $\langle \text{IPR} \rangle \simeq 0$, while localized phases exhibit a significantly larger $\langle \text{IPR} \rangle$. In particular, tuning the relative phase ϕ —which controls the relative strength of the real and imaginary parts of the modulated onsite potential—induces a localization-delocalization transition at different ϕ for $v \in (1, \sqrt{2})$.

For each given pair of parameters (ϕ, v) , the eigenstates are either fully extended or localized. As an illustration, we compute the energy spectrum as a function of ϕ for fixed $v = 1.2$ and mark the fractal dimension Γ of each state. The results are presented in Fig. 3, where 3(a) and 3(b) show the real and imaginary parts of the spectrum, respectively. At $\phi = 0$, all states are extended. As ϕ increases, the states undergo a localization-delocalization transition beyond a critical point, becoming most strongly localized at $\phi = \pi/2$. Upon further increasing ϕ , the system reverts to being extended. This cycle repeats for every shift of ϕ over 2π .

The localization-delocalization transition can be understood from the competition between the quasiperiodic-disorder-induced Anderson localization and NHSEs in the momentum-space Hamiltonian described by Eq. (3). We first consider the Anderson localization aspect by replacing asymmetric couplings with reciprocal couplings $J = \sqrt{|J_+||J_-|}$ upon a similarity transformation. The model in Eq. (3) then becomes the standard AAH model, which belongs to an extended phase for $2t < J$ and a localized phase for $2t > J$, with the Lyapunov exponent $\gamma = \ln(2t/J)$ for all states. When the asymmetric couplings are restored, the phase boundary is determined by comparing γ with the asymmetric ratio $\alpha = \ln[\sqrt{\max(|J_+|, |J_-|)/\min(|J_+|, |J_-|)}]$. For $\gamma > \alpha$ [equivalent to $2t > \max(|J_+|, |J_-|)$], the Anderson localization dominates and all states are localized. For $\gamma < \alpha$ [equivalent to $J < 2t < \max(|J_+|, |J_-|)$], the NHSEs dominate and all states are extended under periodic boundary conditions. Consequently, the system is in an extended phase for $2t < \max(|J_+|, |J_-|)$ and in a localized phase for $2t > \max(|J_+|, |J_-|)$. The phase transition occurs at $2t = \max(|J_+|, |J_-|)$. From this condition, we obtain the phase boundary in (v, ϕ) plane as

$$v = \sqrt{2/(1 + |\sin \phi|)}, \quad (8)$$

i.e., for $v < \sqrt{2/(1 + |\sin \phi|)}$ all eigenstates of the

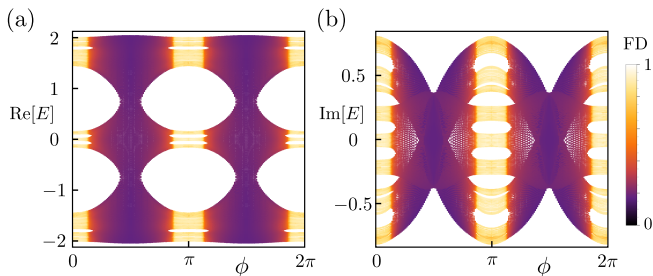


FIG. 3. Energy spectrum as a function of the relative phase shift ϕ , with the fractal dimension Γ of the corresponding eigenstates overlaid. (a) Real parts of the spectrum $\text{Re}(E)$. (b) Imaginary parts of the spectrum $\text{Im}(E)$. The amplitude is fixed at $v = 1.2$. In numerical simulations, the system size is set to $L = F_{15} = 610$.

momentum-space Hamiltonian are localized, while for $v > \sqrt{2/(1 + |\sin \phi|)}$ these eigenstates are all extended. The real-space Hamiltonian exhibits complementary localization behaviors. The dashed line in Fig. 2(a) shows the phase boundary calculated from Eq. (8), which accurately matches the numerical simulation.

B. Topological transitions

Next, we study the topological properties of the system. To characterize the spectral topology, we introduce a magnetic flux Φ into the momentum-space Hamiltonian via a twisted boundary condition. The Hamiltonian in Eq. (3) then becomes

$$H(\Phi) = \sum_{k=1}^{L-1} \left(J_+ b_{k+1}^\dagger b_k + J_- b_k^\dagger b_{k+1} \right) + \sum_{k=1}^L \tilde{V}_k b_k^\dagger b_k + J_+ e^{i\Phi} b_1^\dagger b_L + J_- e^{-i\Phi} b_L^\dagger b_1, \quad (9)$$

where the phase Φ is applied to the boundary hopping terms. The corresponding winding number is then defined as

$$\omega = \frac{1}{2\pi i} \int_0^{2\pi} \partial_\Phi \ln[\det H(\Phi)] d\Phi, \quad (10)$$

which quantifies the spectral winding of the Hamiltonian as Φ varies from 0 to 2π .

The winding number is computed as a function of v and ϕ . The results are shown in Fig. 2(b). The parameter space is divided into three regions: two topological regions with $\omega = \pm 1$ and a trivial region with $\omega = 0$. The topological phase transition from trivial to nontrivial coincides with the transition from extended to localized phases.

The nontrivial topology arises from spectral windings, analogous to those associated with NHSEs. As illustrations, we examine the complex energy spectra for various phase shifts ϕ at fixed $v = 1.2$, where tuning ϕ drives

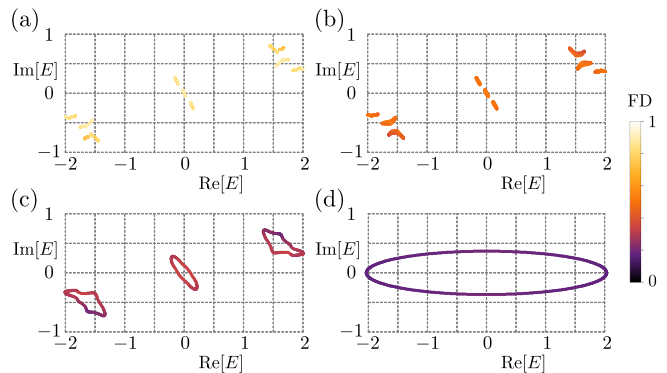


FIG. 4. Complex energy spectra for different relative phase shifts ϕ , with the fractal dimension Γ of the corresponding eigenstates overlaid. (a) $\phi = 0$, (b) $\phi = 0.14\pi$, (c) $\phi = 0.2\pi$, and (d) $\phi = 0.5\pi$. The modulation amplitude is fixed at $v = 1.2$. In numerical simulations, the system size is set to $L = F_{15} = 610$.

a topological phase transition. The results for $\phi = 0, 0.14\pi, 0.2\pi$, and 0.5π are shown in Fig. 3. At $\phi = 0$, the system is topologically trivial, and the complex spectrum forms clusters without loop structures [Fig. 3(a)]. Near the topological phase transition point ($\phi = 0.14\pi$), the spectrum begins to exhibit loop structures, although they remain indistinct [Fig. 3(b)]. Increasing ϕ further into the topological region ($\phi = 0.2\pi$), three main loops emerge in the spectrum [Fig. 3(c)], corresponding to the two main band gaps of the underlying AAH model. As ϕ continues to increase, these loops merge into one, as exemplified by the case with $\phi = 0.5\pi$ in Fig. 3(d).

The topological properties can also be understood from the momentum-space Hamiltonian in Eq. (3). For $v < \sqrt{2/(1 + |\sin \phi|)}$, the momentum-space Hamiltonian is in the localized phase: all states are localized, there is no net current, and consequently the spectral winding number is zero. For $v > \sqrt{2/(1 + |\sin \phi|)}$, the momentum-space Hamiltonian is in the extended phase. The extended nature, combined with asymmetric couplings yields a nonzero spectral winding. Specifically, for $\phi \in (0, \pi)$, we have $|J_+| < |J_-|$ and the spectral winding number $\omega = -1$. For $\phi \in (\pi, 2\pi)$, we have $|J_+| > |J_-|$ and the winding number $\omega = 1$.

C. Degeneracy-breaking transitions

Finally, we examine the degeneracy properties of the system. We define the degeneracy rate as

$$\eta = N_d/N_t, \quad (11)$$

where N_d denotes the number of nearly degenerate states and N_t is the total number of states.

We compute η as a function of v and ϕ , with the results shown in Fig. 2(c). The parameter space is divided into two regions: one in which most states are nearly twofold

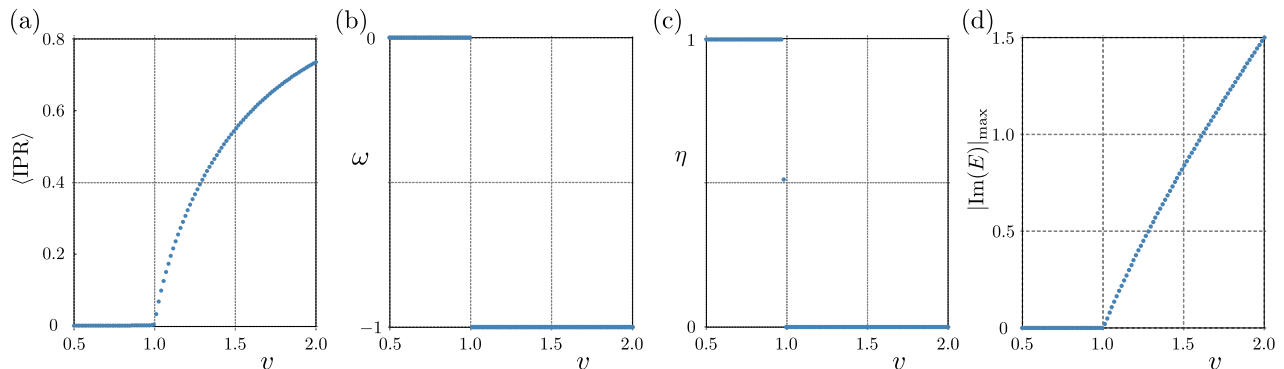


FIG. 5. Topological metal-insulator transitions in the \mathcal{PT} -symmetric case with $\phi = \pi/2$. (a) Localization-delocalization transition: averaged IPR, $\langle \text{IPR} \rangle$, vs v . (b) Topological transition: winding number ω vs v . (c) Degeneracy-breaking transition: degeneracy rate η vs v . (d) \mathcal{PT} transition: maximum imaginary part of eigenenergies $|\text{Im}(E)|_{\text{max}}$ vs v . In numerical simulations, the system size is set to $L = F_{15} = 610$. Two eigenenergies, E_1 and E_2 , are considered degenerate if their distance $|\delta E| \equiv |E_1 - E_2|$ is less than 10^{-5} .

degenerate ($\eta \simeq 1$), and another in which the states are predominantly nondegenerate ($\eta \simeq 0$). The transition between these two regions coincides with the transition from extended to localized phases, as well as with the topological transition from trivial to nontrivial phases, with slight deviations due to finite-size effects.

The degeneracy-breaking transition can be understood by analyzing the momentum-space Hamiltonian in Eq. (3). In the limit $v/t \rightarrow 0$, all states are localized in momentum space. The states $|k_0\rangle$ and $|-k_0\rangle$ are exactly degenerate, forming a degenerate subspace. Extending to the more general localized phase of the momentum-space Hamiltonian, the states $|k_0\rangle$ and $|-k_0\rangle$ are coupled due to exponential localization, leading to an energy splitting approximately given by $\Delta \propto |v|e^{-2|k_0|/\xi}$, where ξ is the localization length. In a quasicrystal of infinite size, most pairs $|k_0\rangle$ and $|-k_0\rangle$ are well separated in momentum space such that $\Delta \rightarrow 0$. Hence, in the localized phase of the momentum-space Hamiltonian, most states are nearly doubly degenerate.

We next consider the opposite limit $t/v \rightarrow 0$, where the system reduces to a 1D uniform chain and all states are extended in momentum space. In the reciprocal case $J_+ = J_-$, most states remain doubly degenerate due to time-reversal symmetry: forward- and backward-propagating modes have identical energies. However, nonreciprocal couplings ($J_+ \neq J_-$) break the time-reversal symmetry and lift the degeneracy. In Hermitian systems, such a degeneracy-breaking can also arise from effective gauge fields that break time-reversal symmetry.

Because the momentum-space and real-space Hamiltonians exhibit complementary localization behaviors, in the extended phase of the real-space Hamiltonian, most states are nearly doubly degenerate, whereas in the localized phase, the states are predominantly non-degenerate.

IV. PHASE TRANSITIONS AT SPECIAL PHASE SHIFTS

We next examine the phase transitions at specific high symmetry points in the parameter space ϕ , i.e., $\phi = m\pi + \pi/2$ and $\phi = m\pi$. At $\phi = m\pi + \pi/2$, the system acquires the \mathcal{PT} symmetry, which introduces an additional real-complex spectral transition alongside the previously discussed triple phase transitions. In contrast, only the localization-delocalization transitions are retained at $\phi = m\pi$.

A. Phase transitions at $\phi = \pi/2$

We use $\phi = \pi/2$ as an example to illustrate the phase transitions at the phase shift $\phi = m\pi + \pi/2$. At $\phi = \pi/2$, the quasiperiodic onsite potential becomes

$$V_n = v_R \cos(2\pi\alpha n) - i v_I \sin(2\pi\alpha n), \quad (12)$$

which satisfies $V_{-n} = V_n^*$. The Hamiltonian H then possesses \mathcal{PT} symmetry.

\mathcal{PT} -symmetric NHQCs could support a triple phase transition, encompassing a localization-delocalization transition, a topological transition, and a \mathcal{PT} -symmetry-breaking transition (or a real-complex spectral transition) simultaneously. Here, we compute the averaged IPR $\langle \text{IPR} \rangle$, the winding number ω , the degeneracy rate η , and the maximum imaginary part of the eigenenergies $|\text{Im}(E)|_{\text{max}}$ as functions of v . The results are presented in Fig. 5. We observe that all phase transitions occur at $v = 1$, as described by Eq. (8). Thus, for \mathcal{PT} -symmetric NHQCs, we find a quartet phase transition, whereas in the general case without \mathcal{PT} symmetry, only a triple phase transition is present.

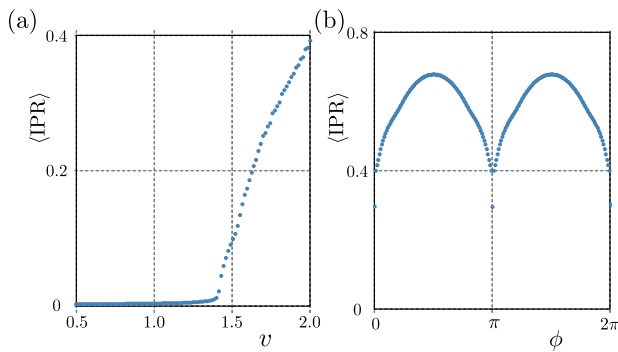


FIG. 6. Localization-delocalization transition for $\phi = 0$. (a) Averaged IPR, $\langle \text{IPR} \rangle$, as a function of v for $\phi = 0$. (b) $\langle \text{IPR} \rangle$ as a function of ϕ for $v = 1.8$. In numerical simulations, the system size is set to $L = F_{15} = 610$.

B. Phase transitions at $\phi = 0$

We use $\phi = 0$ as an example to illustrate the phase transitions at the phase shift $\phi = m\pi$. At $\phi = 0$, we have $J_+ = J_-$, implying the absence of NHSEs even in the extended phase of the momentum-space Hamiltonian. Consequently, no topological phase transitions occur, as evidenced by the vanishing winding number for all v at $\phi = m\pi$ in Fig. 2(b). The condition $J_+ = J_-$ also implies that the time-reversal symmetry is preserved, so that the degeneracy-breaking transition is absent, consistent with $\eta \simeq 1$ for all v at $\phi = m\pi$ in Fig. 2(c). Nevertheless, the localization-delocalization transition remains. To examine this, we compute the averaged IPR, $\langle \text{IPR} \rangle$, as a function of v at $\phi = 0$, with the results shown in Fig. 6(a). A clear change is observed around the phase transition point $v = \sqrt{2}$, consistent with the phase boundary described by Eq. (8). This suggests that two types of localization-delocalization transitions may exist in general NHQCs: one associated with NHSEs and characterized by a topological invariant, and the other unrelated to NHSEs, akin to that in Hermitian systems.

To further illustrate the localization properties of the system, the averaged IPR, $\langle \text{IPR} \rangle$, is computed as a func-

tion of ϕ at a fixed $v = 1.8$. For all ϕ , the system is in localized phases, as indicated by the finite $\langle \text{IPR} \rangle$ values. However, the value of $\langle \text{IPR} \rangle$ at $\phi = m\pi$ is significantly lower than at other values of ϕ , implying a relatively longer localization length in this case.

V. CONCLUSION

We proposed a non-Hermitian quasiperiodic model that generally does not preserve \mathcal{PT} symmetry and demonstrated that the system supports triple phase transitions that involves localization, topology and degeneracy. Both the topological and degeneracy-breaking transitions originate from the NHSEs in momentum space. The system also exhibits a localization transition analogous to the Hermitian case, namely, it occurs without involving a topological or a degeneracy-breaking transition. In most regions of the parameter space, the localization, topological, and degeneracy-breaking transitions take place simultaneously, whereas at special phase shifts, such as $\phi = m\pi$, only localization transitions are present. Our findings not only extend the criterion of localization and topological transitions in NHQCs beyond the perspective of \mathcal{PT} symmetry, but also motivate further experimental investigations of phase transitions in quasicrystal metamaterials, where the relative phase shift between real and imaginary quasiperiodic modulations may serve as a flexible knob to induce and control non-Hermitian phase transitions.

ACKNOWLEDGMENTS

W.Z. and L.Z. acknowledge support by the National Natural Science Foundation of China (Grants No. 12404499, No. 12275260 and No. 11905211). J.G. acknowledges support by the National Research Foundation, Singapore, through the National Quantum Office, hosted in A*STAR, under its Centre for Quantum Technologies Funding Initiative (S24Q2d0009).

-
- [1] M. Kohmoto, Metal-insulator transition and scaling for incommensurate systems, *Phys. Rev. Lett.* **51**, 1198 (1983).
 - [2] S. Das Sarma, S. He, and X. C. Xie, Mobility edge in a model one-dimensional potential, *Phys. Rev. Lett.* **61**, 2144 (1988).
 - [3] H. P. Lüschen, S. Scherg, T. Kohlert, M. Schreiber, P. Bordia, X. Li, S. Das Sarma, and I. Bloch, Single-particle mobility edge in a one-dimensional quasiperiodic optical lattice, *Phys. Rev. Lett.* **120**, 160404 (2018).
 - [4] Y. E. Kraus, Y. Lahini, Z. Ringel, M. Verbin, and O. Zeitlinger, Topological states and adiabatic pumping in quasicrystals, *Phys. Rev. Lett.* **109**, 106402 (2012).
 - [5] Y. E. Kraus and O. Zeitlinger, Topological equivalence between the fibonacci quasicrystal and the harper model, *Phys. Rev. Lett.* **109**, 116404 (2012).
 - [6] L.-J. Lang, X. Cai, and S. Chen, Edge states and topological phases in one-dimensional optical superlattices, *Phys. Rev. Lett.* **108**, 220401 (2012).
 - [7] E. Abrahams, P. W. Anderson, D. C. Licciardello, and T. V. Ramakrishnan, Scaling theory of localization: Absence of quantum diffusion in two dimensions, *Phys. Rev. Lett.* **42**, 673 (1979).
 - [8] J. C. Y. Teo and C. L. Kane, Topological defects and gapless modes in insulators and superconductors, *Phys. Rev. B* **82**, 115120 (2010).

- [9] S. Aubry and G. André, Analyticity breaking and anderson localization in incommensurate lattices, *Ann. Israel Phys. Soc* **3**, 18 (1980).
- [10] D. R. Hofstadter, Energy levels and wave functions of bloch electrons in rational and irrational magnetic fields, *Phys. Rev. B* **14**, 2239 (1976).
- [11] L.-Z. Tang, S.-N. Liu, G.-Q. Zhang, and D.-W. Zhang, Topological anderson insulators with different bulk states in quasiperiodic chains, *Phys. Rev. A* **105**, 063327 (2022).
- [12] Z. L. Y. Z. Z. Xu, Reentrant localization transitions in a topological anderson insulator: A study of a generalized su schrieffer heeger quasicrystal, *Front. Phys.* **20**, 024204 (2025).
- [13] X. Li, H. Xu, J. Wang, L.-Z. Tang, D.-W. Zhang, C. Yang, T. Su, C. Wang, Z. Mi, W. Sun, X. Liang, M. Chen, C. Li, Y. Zhang, K. Linghu, J. Han, W. Liu, Y. Feng, P. Liu, G. Xue, J. Zhang, Y. Jin, S.-L. Zhu, H. Yu, S. P. Zhao, and Q.-K. Xue, Mapping the topology-localization phase diagram with quasiperiodic disorder using a programmable superconducting simulator, *Phys. Rev. Res.* **6**, L042038 (2024).
- [14] I. Mondragon-Shem, T. L. Hughes, J. Song, and E. Prodan, Topological criticality in the chiral-symmetric aiii class at strong disorder, *Phys. Rev. Lett.* **113**, 046802 (2014).
- [15] E. J. Meier, F. A. An, A. Dauphin, M. Maffei, P. Massignan, T. L. Hughes, and B. Gadway, Observation of the topological anderson insulator in disordered atomic wires, *Science* **362**, 929 (2018).
- [16] M. Ren, X. Shi, H. Jiang, F. Liu, H. Chen, and Y. Sun, Anomalous non-hermitian topological anderson insulator, *Phys. Rev. B* **113**, 064202 (2026).
- [17] Y. Ashida, Z. Gong, and M. Ueda, Non-hermitian physics, *Adv. Phys.* **69**, 249 (2020).
- [18] E. J. Bergholtz, J. C. Budich, and F. K. Kunst, Exceptional topology of non-hermitian systems, *Rev. Mod. Phys.* **93**, 015005 (2021).
- [19] L. Zhou and D.-J. Zhang, Non-hermitian floquet topological matter—a review, *Entropy* **25**, 1401 (2023).
- [20] R. Lin, T. Tai, L. Li, and C. H. Lee, Topological non-hermitian skin effect, *Front. Phys.* **18**, 53605 (2023).
- [21] S. Yao and Z. Wang, Edge states and topological invariants of non-hermitian systems, *Phys. Rev. Lett.* **121**, 086803 (2018).
- [22] V. M. Martinez Alvarez, J. E. Barrios Vargas, and L. E. F. Foa Torres, Non-hermitian robust edge states in one dimension: Anomalous localization and eigenspace condensation at exceptional points, *Phys. Rev. B* **97**, 121401 (2018).
- [23] F. K. Kunst, E. Edvardsson, J. C. Budich, and E. J. Bergholtz, Biorthogonal bulk-boundary correspondence in non-hermitian systems, *Phys. Rev. Lett.* **121**, 026808 (2018).
- [24] C. H. Lee and R. Thomale, Anatomy of skin modes and topology in non-hermitian systems, *Phys. Rev. B* **99**, 201103 (2019).
- [25] K. Kawabata and S. Ryu, Nonunitary scaling theory of non-hermitian localization, *Phys. Rev. Lett.* **126**, 166801 (2021).
- [26] X. Luo, T. Ohtsuki, and R. Shindou, Transfer matrix study of the anderson transition in non-hermitian systems, *Phys. Rev. B* **104**, 104203 (2021).
- [27] X. Luo, T. Ohtsuki, and R. Shindou, Universality classes of the anderson transitions driven by non-hermitian disorder, *Phys. Rev. Lett.* **126**, 090402 (2021).
- [28] Z. Chen, K. Kawabata, A. Kulkarni, and S. Ryu, Field theory of non-hermitian disordered systems, *Phys. Rev. B* **111**, 054203 (2025).
- [29] N. Hatano and D. R. Nelson, Localization transitions in non-hermitian quantum mechanics, *Phys. Rev. Lett.* **77**, 570 (1996).
- [30] A. A. Asatryan, N. A. Nicorovici, P. A. Robinson, C. M. de Sterke, and R. C. McPhedran, Electromagnetic localization in one-dimensional stacks with random loss and gain, *Phys. Rev. B* **54**, 3916 (1996).
- [31] J. Feinberg and A. Zee, Non-hermitian localization and delocalization, *Phys. Rev. E* **59**, 6433 (1999).
- [32] K. Kawabata, K. Shiozaki, M. Ueda, and M. Sato, Symmetry and topology in non-hermitian physics, *Phys. Rev. X* **9**, 041015 (2019).
- [33] H. Zhou and J. Y. Lee, Periodic table for topological bands with non-hermitian symmetries, *Phys. Rev. B* **99**, 235112 (2019).
- [34] C.-H. Liu and S. Chen, Topological classification of defects in non-hermitian systems, *Phys. Rev. B* **100**, 144106 (2019).
- [35] A. Jazaeri and I. I. Satija, Localization transition in incommensurate non-hermitian systems, *Phys. Rev. E* **63**, 036222 (2001).
- [36] Q.-B. Zeng, S. Chen, and R. Lü, Anderson localization in the non-hermitian aubry-andré-harper model with physical gain and loss, *Phys. Rev. A* **95**, 062118 (2017).
- [37] H. Jiang, L.-J. Lang, C. Yang, S.-L. Zhu, and S. Chen, Interplay of non-hermitian skin effects and anderson localization in nonreciprocal quasiperiodic lattices, *Phys. Rev. B* **100**, 054301 (2019).
- [38] S. Longhi, Metal-insulator phase transition in a non-hermitian aubry-andré-harper model, *Phys. Rev. B* **100**, 125157 (2019).
- [39] Q.-B. Zeng, Y.-B. Yang, and Y. Xu, Topological phases in non-hermitian aubry-andré-harper models, *Phys. Rev. B* **101**, 020201 (2020).
- [40] X. Cai, Boundary-dependent self-dualities, winding numbers, and asymmetrical localization in non-hermitian aperiodic one-dimensional models, *Phys. Rev. B* **103**, 014201 (2021).
- [41] L.-Z. Tang, G.-Q. Zhang, L.-F. Zhang, and D.-W. Zhang, Localization and topological transitions in non-hermitian quasiperiodic lattices, *Phys. Rev. A* **103**, 033325 (2021).
- [42] Y. Liu, Q. Zhou, and S. Chen, Localization transition, spectrum structure, and winding numbers for one-dimensional non-hermitian quasicrystals, *Phys. Rev. B* **104**, 024201 (2021).
- [43] X. Cai, Localization and topological phase transitions in non-hermitian aubry-andré-harper models with p -wave pairing, *Phys. Rev. B* **103**, 214202 (2021).
- [44] S. Longhi, Non-hermitian maryland model, *Phys. Rev. B* **103**, 224206 (2021).
- [45] S. Longhi, Phase transitions in a non-hermitian aubry-andré-harper model, *Phys. Rev. B* **103**, 054203 (2021).
- [46] A. P. Acharya, A. Chakrabarty, D. K. Sahu, and S. Datta, Localization, \mathcal{PT} symmetry breaking, and topological transitions in non-hermitian quasicrystals, *Phys. Rev. B* **105**, 014202 (2022).
- [47] L. Zhou and Y. Gu, Topological delocalization transitions and mobility edges in the nonreciprocal maryland model, *J. Phys.: Condens. Matter* **34**, 115402 (2022).

- [48] X. Cai, Localization transitions and winding numbers for non-hermitian aubry-andré-harper models with off-diagonal modulations, *Phys. Rev. B* **106**, 214207 (2022).
- [49] L.-M. Chen, Y. Zhou, S. A. Chen, and P. Ye, Quantum entanglement of non-hermitian quasicrystals, *Phys. Rev. B* **105**, L121115 (2022).
- [50] T. Orito and K.-I. Imura, Unusual wave-packet spreading and entanglement dynamics in non-hermitian disordered many-body systems, *Phys. Rev. B* **105**, 024303 (2022).
- [51] L. Zhou, Entanglement phase transitions in non-hermitian quasicrystals, *Phys. Rev. B* **109**, 024204 (2024).
- [52] S.-Z. Li, X.-J. Yu, and Z. Li, Emergent entanglement phase transitions in non-hermitian aubry-andré-harper chains, *Phys. Rev. B* **109**, 024306 (2024).
- [53] X. Zhu, T. Peng, F. Lyu, W. Cao, Y. Hou, R. Xiong, and Z. Wang, Non-hermitian quasicrystalline topological insulators, *Phys. Rev. B* **111**, 035305 (2025).
- [54] S. Gandhi and J. N. Bandyopadhyay, Topological in-gap states in a non-hermitian quasicrystal with p -wave pairing, *Phys. Rev. B* **112**, 104201 (2025).
- [55] Q.-B. Zeng and Y. Xu, Winding numbers and generalized mobility edges in non-hermitian systems, *Phys. Rev. Res.* **2**, 033052 (2020).
- [56] Y. Liu, X.-P. Jiang, J. Cao, and S. Chen, Non-hermitian mobility edges in one-dimensional quasicrystals with parity-time symmetry, *Phys. Rev. B* **101**, 174205 (2020).
- [57] T. Liu, H. Guo, Y. Pu, and S. Longhi, Generalized aubry-andré self-duality and mobility edges in non-hermitian quasiperiodic lattices, *Phys. Rev. B* **102**, 024205 (2020).
- [58] L. Zhou, Floquet engineering of topological localization transitions and mobility edges in one-dimensional non-hermitian quasicrystals, *Phys. Rev. Res.* **3**, 033184 (2021).
- [59] L. Zhou and W. Han, Non-hermitian quasicrystal in dimerized lattices, *Chin. Phys. B* **30**, 100308 (2021).
- [60] Z.-H. Wang, F. Xu, L. Li, D.-H. Xu, and B. Wang, Unconventional real-complex spectral transition and majorana zero modes in nonreciprocal quasicrystals, *Phys. Rev. B* **104**, 174501 (2021).
- [61] Z. Xu, X. Xia, and S. Chen, Non-hermitian aubry-andré model with power-law hopping, *Phys. Rev. B* **104**, 224204 (2021).
- [62] Y. Liu, Y. Wang, X.-J. Liu, Q. Zhou, and S. Chen, Exact mobility edges, \mathcal{PT} -symmetry breaking, and skin effect in one-dimensional non-hermitian quasicrystals, *Phys. Rev. B* **103**, 014203 (2021).
- [63] W. Han and L. Zhou, Dimerization-induced mobility edges and multiple reentrant localization transitions in non-hermitian quasicrystals, *Phys. Rev. B* **105**, 054204 (2022).
- [64] Y. Liu, Y. Wang, Z. Zheng, and S. Chen, Exact non-hermitian mobility edges in one-dimensional quasicrystal lattice with exponentially decaying hopping and its dual lattice, *Phys. Rev. B* **103**, 134208 (2021).
- [65] C. Yuce and H. Ramezani, Coexistence of extended and localized states in the one-dimensional non-hermitian anderson model, *Phys. Rev. B* **106**, 024202 (2022).
- [66] X. Xia, K. Huang, S. Wang, and X. Li, Exact mobility edges in the non-hermitian t_1-t_2 model: Theory and possible experimental realizations, *Phys. Rev. B* **105**, 014207 (2022).
- [67] L. Zhou and W. Han, Driving-induced multiple \mathcal{PT} -symmetry breaking transitions and reentrant localization transitions in non-hermitian floquet quasicrystals, *Phys. Rev. B* **106**, 054307 (2022).
- [68] L. Zhou, Non-abelian generalization of non-hermitian quasicrystals: \mathcal{PT} -symmetry breaking, localization, entanglement, and topological transitions, *Phys. Rev. B* **108**, 014202 (2023).
- [69] L. Wang, Z. Wang, and S. Chen, Non-hermitian butterfly spectra in a family of quasiperiodic lattices, *Phys. Rev. B* **110**, L060201 (2024).
- [70] T. Qian, Y. Gu, and L. Zhou, Correlation-induced phase transitions and mobility edges in an interacting non-hermitian quasicrystal, *Phys. Rev. B* **109**, 054204 (2024).
- [71] Q. Tang and Y. He, Mobility edges in non-hermitian models with slowly varying quasiperiodic disorder, *Phys. Rev. B* **109**, 224204 (2024).
- [72] Y. Zhang and L. Zhou, Two-body interaction induced phase transitions and intermediate phases in nonreciprocal non-hermitian quasicrystals, *Phys. Rev. B* **111**, 064204 (2025).
- [73] S. Longhi, Topological phase transition in non-hermitian quasicrystals, *Phys. Rev. Lett.* **122**, 237601 (2019).
- [74] S. Weidemann, M. Kremer, S. Longhi, and A. Szameit, Topological triple phase transition in non-hermitian floquet quasicrystals, *Nature* **601**, 354 (2022).
- [75] Q. Lin, T. Li, L. Xiao, K. Wang, W. Yi, and P. Xue, Topological phase transitions and mobility edges in non-hermitian quasicrystals, *Phys. Rev. Lett.* **129**, 113601 (2022).